Pergamon

PII: S0301-9322(96)00018-3

Int. J. Multiphase Flow Vol. 22, No. 4, pp. 797–805, 1996

0301-9322/96 $15.00 + 0.00

NUMERICAL RESULTS AND DESIGNING ASPECTS CONCERNING THE HGMF FILTERING CELLS WITH BOUND FLOW FIELD

V. BADESCU, O. ROTARIU, V. MURARIU AND N. REZLESCU
Institute of Technical Physics, Bd. Mangeron 47, R-6600 Iasi, Romania

(Received 26 December 1995; in revised form 13 March 1996)

Abstract—The work presents analytical and numerical results and some designing aspects concerning the high gradient magnetic filtration (HGMF) of fine paramagnetic particles of a fluid suspension flowing through bound spaces. Our analysis concerns two HGMF systems, in axial and transversal configurations respectively, with the ferromagnetic wires placed outside the flow field. The conditions of maximum recovery of particles are established for these systems. The obtained results can be used to design magnetic filtering systems with anticorrosive and antierosive protection of the ferromagnetic wires. Copyright © 1996 Elsevier Science Ltd.

Key Words: magnetic filtration, paramagnetic particles, fluid suspensions, laminar flow

1. INTRODUCTION

The high gradient magnetic filtration (HGMF) is a physical method for filtering the fine particles from fluid suspensions. Based on the magnetic particles captures on ferromagnetic wires magnetised by an external magnetic field applied perpendicularly to their axes (Watson 1973; Oberteuffer 1974) this method has multiple applications in treating and filtering the industrial waste waters (Elliott *et al.* 1979; Sushil *et al.* 1979). Preoccupied by the realization of the anticorrosive and antierosive protection of the ferromagnetic wires and by getting a maximum filtration efficiency, Badescu *et al.* (1995a,b) have initiated the analysis of some HGMF magnetic filtering systems in which the fluid suspensions are flowing through bound spaces having ferromagnetic wires with circular cross section mounted outside them.

We present in this work the main analytical and numerical results obtained by analysing two types of magnetic filtration cells with bound flow field, one in HGMF axial configuration and the other in HGMF transversal configuration. The analysis is based on the study of the particles' trajectories and has resulted in establishing the conditions for a 100% filtration efficiency. The obtained results have been used for designing two practical devices for magnetic filtration whose schematic diagrams are presented at the end of the work.

2. DESCRIPTION OF THE ANALYSED SYSTEMS

Figure 1(a) presents the filtration cell in the case of the axial HGMF configuration. A cylindrical tube with the radius R bounds the flow field of a fluid suspension consisting of fine paramagnetic particles of radius b and magnetic susceptibility χ, in a fluid with the viscosity η_f. Outside the tube and parallel with its axis a cylindrical ferromagnetic wire is mounted of radius, a, length l and saturation magnetization M_s. A magnetic field of the strength H_0 is applied perpendicularly to the ferromagnetic wire axis; the fluid suspension flows with the average velocity v_0.

The filtration cell in HGMF transversal configuration is presented in figure 1(b). It consists of two plane plates parallel to each other and to the plane $x_a = 0$, at the distance $x_a = d_{1a} = d_1/a$ and $x_a = 2d_{1a} + h_a$, where $h_a = h/a$, and two groups of n cylindrical ferromagnetic wires, parallel to each other and separated by the distance $d_a = d/a$ between the axes, having the radius of their cross section a and infinite length. The wires from the first group are coplanar in the plane $x_a = 0$, and those from the second group—in the plane $x_a = 2d_{1a} + h_a$, the two groups being shifted along the Oy_a axis by the distance $d_{2a} = d_2/a$. The background magnetic field H_0 is directed along the Ox_a

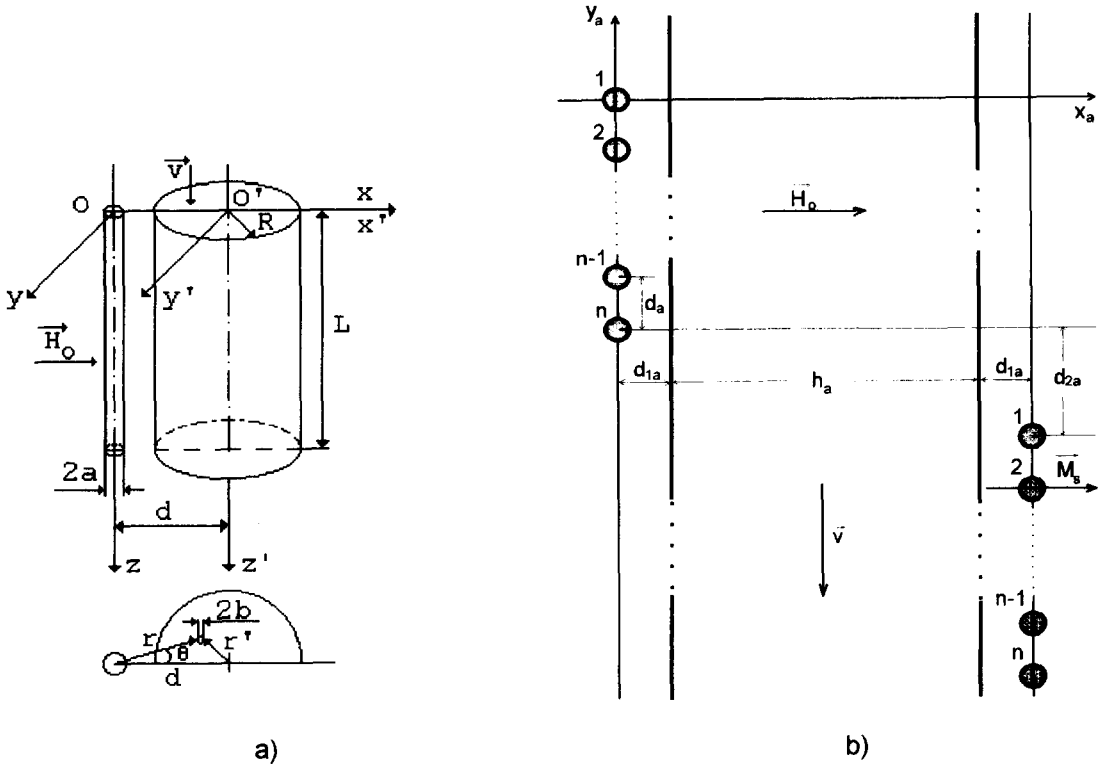

Figure 1. Schematic diagrams of the analysed systems: (a) the HGMF axial configuration; (b) the HGMF transversal configuration.

axis, and the fluid suspension flows in a direction opposite to the Oy_a axis.

3. ANALYTICAL AND NUMERICAL RESULTS

3.1. The HGMF axial configuration

In the case of the axial configuration, the trajectories of the solid particles in suspension are given by the following equations (Badescu *et al.* 1995a):

$$r_a^2 = C \sin 2(\theta - \alpha) \qquad [1]$$

$$z_a = \frac{v_0}{v_m}\frac{2}{R_a^2}\left[C^3 I_1(\theta) + C^2(d_a^2 - R_a^2) I_2(\theta) - 2 d_a C^{5/2} I_3(\theta) \right]. \qquad [2]$$

In [1], C and α are two constants depending on r_{a0} and θ_0, the values of r_a and θ at the entrance in the magnetically active space. Except for the case when $\sin 2\theta_0 = 0$, which in the analysed system corresponds to $\theta_0 = 0$, they have the expressions:

$$C = \frac{(r_{a_0}^4 + 2K^2 r_{a_0}^2 \cos 2\theta_0 + K)^{1/2}}{\sin 2\theta_0} \qquad [3]$$

$$\alpha = \frac{1}{2}\arctan\frac{K \sin 2\theta_0}{r_{a_0}^4 + K \cos 2\theta_0} \qquad [4]$$

where $K = M_s/2H_0$ for $H_0 > M_s/2$ and $K = 1$ for $H_0 < M_s/2$, and $v_m = 2\mu_0 \chi H_0 M_s b^2/9\eta_f a$ is a factor with the dimension of a velocity and is called "magnetic velocity" (it also stands for the final velocity of a particle under the simultaneous actions of the magnetic and drag forces).

In [2], $I_1(\theta)$, $I_2(\theta)$ and $I_3(\theta)$ are functions given by:

$$I_1(\theta) = \int_{\theta_0}^{\theta} \sin^2 2\theta \, d\theta = \tfrac{1}{2}(\theta - \theta_0) - \tfrac{1}{8}(\sin 4\theta - \sin 4\theta_0) \qquad [5]$$

$$l_2(\theta) = \int_{\theta_0}^{\theta} \sin 2\theta \, \mathrm{d}\,\theta = -\tfrac{1}{2}(\cos 2\theta - \cos 2\theta_0) \qquad [6]$$

$$l_3(\theta) = \int_{\theta_0}^{\theta} \cos\theta(\sin 2\theta)^{3/2} \, \mathrm{d}\,\theta = \frac{3}{16}\arctan\frac{(1-\tan\theta_0)\sqrt{2\tan\theta} - (1-\tan\theta)\sqrt{2\tan\theta_0}}{(1-\tan\theta)(1-\tan\theta_0) + 2\sqrt{\tan\theta\,\tan\theta_0}}$$
$$+ \frac{3}{32}\ln\frac{(1+\tan\theta+\sqrt{2\tan\theta})(1+\tan\theta_0-\sqrt{2\tan\theta_0})}{(1+\tan\theta-\sqrt{2\tan\theta})(1+\tan\theta_0+\sqrt{2\tan\theta_0})}$$
$$+ \cos^2\theta\sqrt{\frac{\tan\theta}{2}}\left(\frac{1}{4}-\cos^2\theta\right) - \cos^2\theta_0\sqrt{\frac{\tan\theta_0}{2}}\left(\frac{1}{4}-\cos^2\theta_0\right). \qquad [7]$$

In the case that $\theta_0 = 0$, θ remains zero all along the trajectory and the equation of trajectory in the (x, z) plane is:

$$z_a = \frac{v_0}{v_m}\frac{2}{R_a^2}\left[(d_a^2 - R_a^2)J_1(r_a) - 2d_aJ_2(r_a) + J_3(r_a)\right] \qquad [8]$$

where

$$J_1(r_a) = \int_{r_{a_0}}^{r_a} \frac{r_a^5}{K+r_a^2}\,\mathrm{d}\,r_a = \frac{1}{4}[r_a^4 - r_{a_0}^4) - \frac{K}{2}(r_a^2 - r_{a_0}^2) + \frac{K^2}{2}\ln\frac{K+r_a^2}{K+r_{a_0}^2} \qquad [9]$$

$$J_2(r_a) = \int_{r_{a_0}}^{r_a} \frac{r_a^6}{K+r_a^2}\,\mathrm{d}\,r_a = \frac{1}{5}\left(r_a^5 - r_{a_0}^5\right) - \frac{K}{3}\left(r_a^3 - r_{a_0}^3\right)$$
$$+ K^2(r_a - r_{a_0}) - K^{5/2}\left(\arctan\frac{r_a}{\sqrt{K}} - \arctan\frac{r_{a_0}}{\sqrt{K}}\right) \qquad [10]$$

$$J_3(r_a) = \int_{r_{a_0}}^{r_a} \frac{r_a^7}{K+r_a^2}\,\mathrm{d}\,r_a = \frac{1}{6}\left(r_a^6 - r_{a_0}^6\right) - \frac{K}{4}\left)r_a^4 - r_{a_0}^4 + \frac{K^2}{2}\left(r_a^2 - r_{a_0}^2\right) - \frac{K^3}{2}\ln\frac{K+r_a^2}{K+r_{a_0}^2}. \qquad [11]$$

Figure 2(a) presents four trajectories for four sets of initial conditions, and figure 2(b) presents their projections in the (r, θ) plane. The trajectory of a paramagnetic particle will intersect the tube

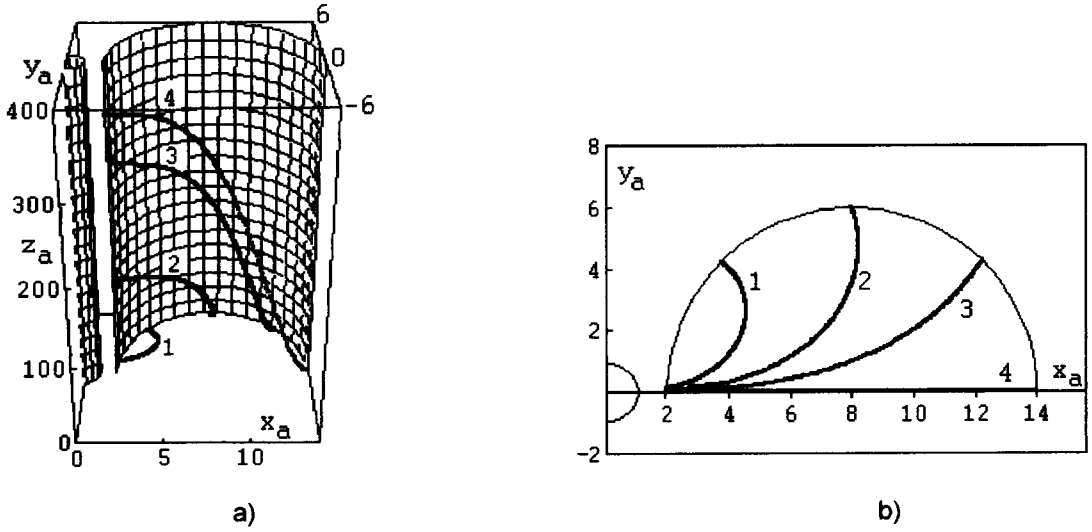

Figure 2. (a) Trajectories of the particles for the HGMF axial configuration; (b) trajectory projections in the (r, θ) plane. The initial conditions namely in the $O'x'y'z'$ reference system are: $r_0' = R$ and $\theta_0' = \pi/4$ (curve 1), $\theta_0' = \pi/2$ (2), $\theta_0' = 3\pi/4$ (3), $\theta_0' = 0$ (4).

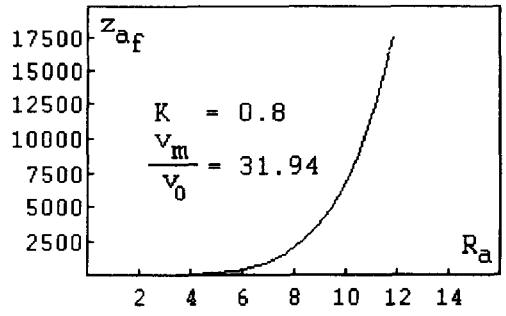

Figure 3. Dependence of z_{a_f} vs R_a when $r_{a_0} = R_a + d_a$ and $\theta_0 = 0$.

surface at a point whose coordinates r_{a_f} and θ_f are given by

$$r_{a_f} \approx d_a - R_a \qquad [12]$$

$$\theta_f \approx \frac{1}{2}\arcsin\left[\frac{(d_a - R_a)^2}{C}\right]. \qquad [13]$$

The relations [12] and [13] together with [2] and [8] enable the determination of the final coordinate z_{a_f} of the particle. Figure 3 presents the dependence of z_{a_f} on the tube radius R_a for $K = 0.8$ and $v_m/v_0 = 31.94$. A monotoneous increase of z_{a_f} with R_a can be noticed.

In order to estimate the efficiency of a filtration cell, we drew the isotelic curves and calculated the capture cross sections corresponding to them. For the calculation of the isotelic curves we used the normalized captured length defined as

$$L_{a_c} = \frac{v_m}{v_0} z_{a_f}. \qquad [14]$$

This variable includes all the specific parameters of a filtration cell, both constructive (L, R, d, a, M_s) and operational (b, χ, v_0, η, H_0). Finally, it permits us to evaluate the effect of each of these parameters on the filtration efficiency. The isotelic curve is the geometric locus of all the points of emergence in the magnetically active space for which the capture length has a constant value. The capture cross-section area is bound by the sector of the tube wall next to the ferromagnetic wire and the isotelic curve corresponding to a normalized capture length L_{a_c}.

Figure 4(a) presents a family of isotelic curves for different constructive and operational parameters of the cell. One can notice that, by changing these parameters, we can increase the capture cross-section area bound by the isotelic curves until it includes the cross section of the cell tube, which corresponds to a 100% recovery. Figure 4(b) presents the dependence of the ratio between the capture cross-section area and the tube cross-section area, on the normalized capture length, for the same parameters as in figure 4(a). One can remark that in this case there is a

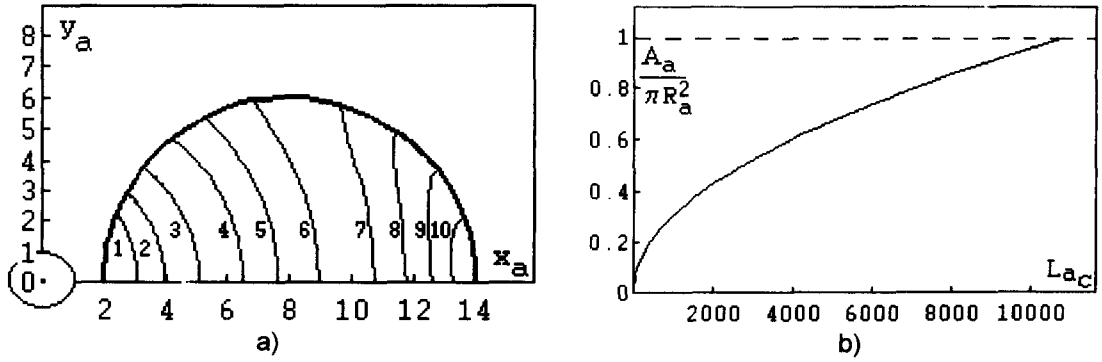

Figure 4. (a) A family of isotelic curves for the following parameters: $K = 0.8$, $R_a = 6$, $d_a = 8$ and $L_{ac} = 10$ (curve 1), 50(2), 300(3), 700(4), 1500(5), 3000(6), 6000(7), 8000(8), 9500(9), 10500(10); (b) the normalized capture length dependence on the ratio between the capture cross-section area and the tube cross-section area.

Table 1

a (mm)	L (mm)	R (mm)	d (mm)	M_s (kA/m)	b (μm)	$\chi \times 10^3$ (u.Sl)	λ_f (Kg/ms)	v_0 (cms.s)	H_0 (kA.m)
1.0	500.0	5.0	7.0	1600.0	16.0	3.14	0.001	1.0	320.0
1.0	550.0	5.0	7.0	1600.0	16.0	3.14	0.001	2.5	820.0
1.0	300.0	5.0	7.0	1600.0	16.0	3.14	0.001	1.0	540.0
1.0	300.0	5.0	7.0	1600.0	16.0	3.14	0.001	2.5	1400.0

value L_{a_c} for which this ratio equals unity. Under these circumstances, the filtration cell recovery is 100%.

In table 1 are presented four sets of constructive and operational parameters of the HGMF-axial analysed cell for which the recovery is 100%.

3.2. The HGMS transversal configuration

In the case of the transversal configuration, the equation of the trajectory of a particle in suspension has the following analytical expression (Badescu *et al.* 1995b)

$$U = \frac{3}{2}x_a - 2h_a\left(\frac{x_a}{h_a} - \frac{d_{1a}}{h_a} - \frac{1}{2}\right)^3 - \frac{v_m}{v_0}\left[\sum_{j=1}^{n}\frac{x_a y_{aj}}{(x_a^2 + y_{aj}^2)^2} + \sum_{j=1}^{n}\frac{(x_a - 2d_{1a} - h_a)[y_{aj} + (n-1)d_a + d_{2a}]}{\{(x_a - 2d_{1a} - h_a)^2 + [y_{aj} + (n-1)d_a + d_{2a}]^2\}^2}\right] = \frac{\text{Const}}{v_0} \quad [15]$$

where

$$y_{aj} = y_a + (j-1)d_a. \quad [16]$$

In order to evaluate the efficiency of the system, we have followed the particles' trajectories by numerically solving [15]. The coordinates of the initial points of the obtained trajectories were $d_{1a} > x_a^i > (d_{1a} + h_a)$ and $y_a^i = 100$. Depending on the values of the constructive and operational parameters of the system and of the initial coordinate $x_a^i$of a particle, this can or can not be captured on one of the two planes bounding the flow. We have noticed the existence of the critical trajectories, and points, the number of the last ones being equal to the number of wires in the system. Figure 5(a) presents a set of critical trajectories for a system of $2 \times n = 6$ wires, taking into account the following parameters of the system: $2 \times n = 6$, $d_a = 4$, $d_{1a} = 1.5$, $d_{2a} = 20$, $v_m/v_0 = 50$, $h_a = 10$. One must remark the presence of an inactive zone of the system, situated between the critical trajectories corresponding to the 3rd and 6th wires, a zone where the particles are not captured. In this case, the filtration efficiency of the system is lower than 100%. Yet, when reducing the distance between the walls bounding the flow down to $h_a = 6.7$, for the same value of the other parameters, the disappearance of the inactive zone is noticed, the efficiency of the system becoming 100% (see figure 5(b)).

By noting with h_a^{100} the distance separating the walls that bound the flow, for which the filtration efficiency is 100%, we have numerically studied the dependence of this parameter on the other system's parameters. The results are presented in figure 6. One can see that the cross section of the flow tube bound by the two walls increases with v_m/v_0, the increase being the higher the closer are the ferromagnetic wires in the two groups. At the same time, an increase of h_a^{100} with the number of wires in each group is noticed, this increase being maximum when d_a is minimum.

In table 2 are presented four sets of constructive and operational parameters of the HGMF-transversal analysed cell for which the filtration efficiency is 100%.

4. MAGNETIC FILTERS DESIGNS

The results obtained and presented in the previous sections enabled the designing of magnetic filtration devices that can work in maximum recovery regime, both in axial and transversal configuration.

Thus, in the axial configuration [figure 7(a–c)] the magnetic filter includes an assembly of double capture cells, each cell consisting of a cylindrical ferromagnetic wire 1 of the radius a and two cylindrical tubings 2 and 2′ of radius R, all three having the length L and being mounted with

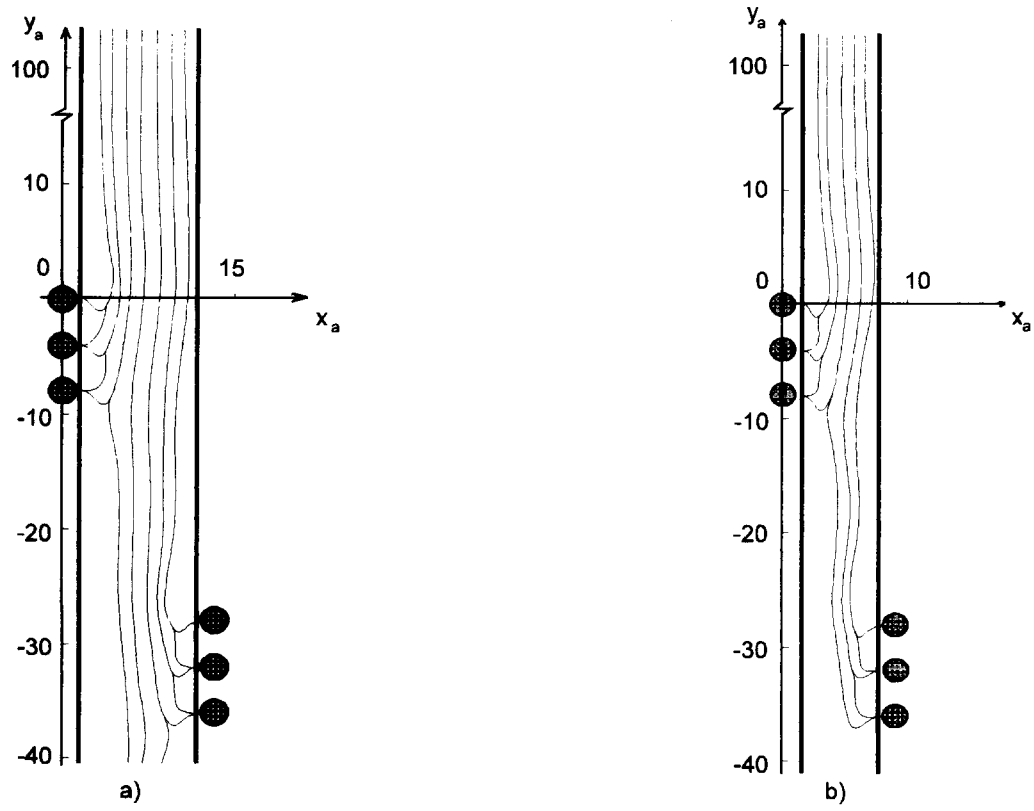

Figure 5. Critical trajectories of the particles for the HGMF transversal configuration with the following parameters: $2 \times n = 6$, $d_a = 4$, $d_{1a} = 1.5$, $d_{2a} = 20$, $v_m/v_0 = 50$; (a) $h_a = 10$, recovery $< 100\%$; (b) $h_a = 6.7$, recovery $= 100\%$.

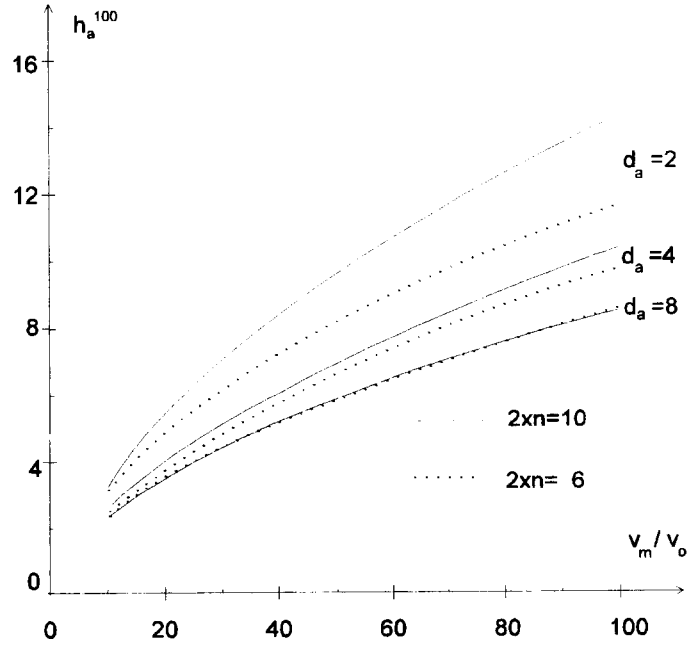

Figure 6. The dependence of the distance h_a^{100} separating the planes that restrict the flow for 100% recovery, on v_m/v_0 ratio.

Table 2

a (mm)	d (mm)	d_1 (mm)	d_2 (mm)	n	h^{100} (mm)	M_s (kA.m)	b (μm)	$\chi \times 10^3$ (u.Sl)	v_f (Kg/ms)	v_0 (cm/s)	H_0 (kA/m)
1.0	4.0	1.5	20.0	3	5.0	1600.0	16.0	3.14	0.001	1.0	835.0
1.0	4.0	1.5	20.0	3	3.5	1600.0	16.0	3.14	0.001	2.5	1200.0
1.0	4.0	1.5	20.0	5	6.0	1600.0	16.0	3.14	0.001	1.0	1115.0
1.0	4.0	1.5	20.0	5	4.0	1600.0	16.0	3.14	0.001	2.5	1400.0

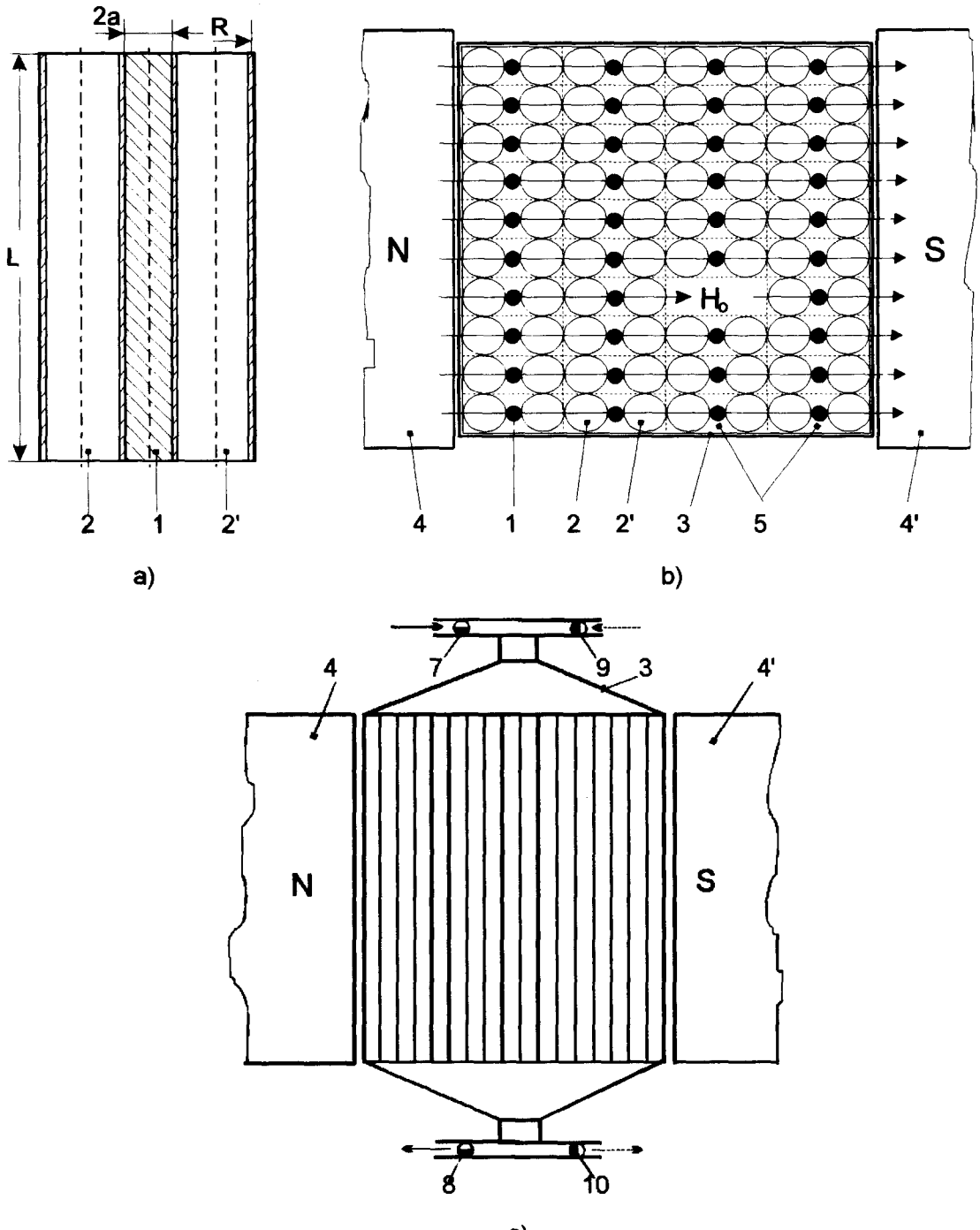

Figure 7. Schematic diagrams of the magnetic filter design for the HGMF axial configuration: (a) double capture cell; (b) cross section; (c) longitudinal section.

coplanar axes [figure 7(a)]. The capture cells are orderly assembled and closed in the enclosure 3, this one being place between the poles 4 and 4′ of an electromagnet. The space outside the tubings of the assembly of capture cells is filled with an adequate filling material 5. In the cross sections, the capture cells are orderly distributed, with the ferromagnetic wires 1 in parallel planes placed perpendicularly to the lines of the magnetic field H_0 generated by the electromagnet [figure 7(b)]. Both the constructive parameters, i.e. the radii a and R and the length L, and the operational parameters, i.e. the strength H_0 of the applied magnetic field and the flow velocity v_0 of the filtered suspension through the capture cell tubings, determine the capture cross section area. During the operation the operational parameters are adjusted so that the capture cross section of every cell includes the cross sections of the two tubes composing it. Both the distribution of the cells inside the filter and an adequate choice of specific parameters eliminate the overlapping of the cross sections of the joining capture cells.

The operation of the magnetic filter is cyclical. In the presence of the magnetic field, the suspension to be filtered is introduced by means of the tap 7 and the filtered carrier fluid is evacuated through the tap 8. In time, the filter is loaded with captured solid particles that make stable buildups inside the tubings on the sectors joining the ferromagnetic wires of every cell. After the saturation the taps 7 and 8 are turned off and the magnetic field intensity is reduced to zero, the filter being washed with clean fluid introduced through the tap 9 and then evacuated together with the material taken over, through the tap 10 [figure 7(c)]. The two stages alternate cyclically.

In the case of the transversal configuration, the magnetic filter [figure 8(a, b)] includes an assembly of pairs of plane parallel walls, bounding the current tubes 2 in the flow field of the suspension to be filtered. On the external faces of the walls 1, outside the flow field, are sticked groups of 2, 3, 4 . . . cylindrical ferromagnetic wires 3, parallel and equispaced, the groups being placed alternatively on the two sides of the stream tube. The empty spaces between the ferromagnetic wires outside the flow field are filled with an adequate filling material 4. All this assembly is closed in a parallelepipedic enclosure 5 [figure 8(b)]. The enclosure 5 is placed, in turn, between the poles, 6, 6′ of an electromagnet.

The constructive parameters, the ferromagnetic wire radii, the width of each stream tube, the distance separating two joining wires and the shift between two successive wires groups as well as the working parameters: the strength of the applied magnetic field and the flow velocity of the

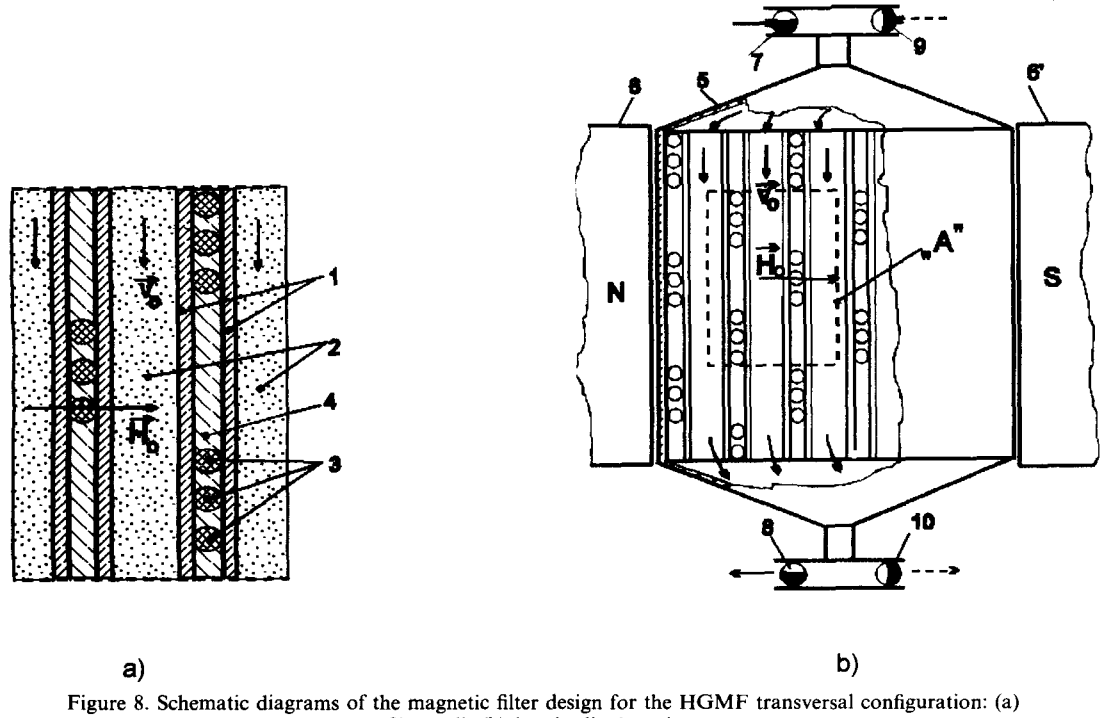

Figure 8. Schematic diagrams of the magnetic filter design for the HGMF transversal configuration: (a) filter cell; (b) longitudinal section.

suspension to be filtered determine the capture cross area. During the operation, the working parameters are adjusted so that the cross section area of the flow field between to walls is equal or smaller than the captured cross section area of the whole assembly of ferromagnetic wires sticked outside the two walls, this enabling to get a 100% filtering efficiency. The operation of the HGMF transversal filter is also cyclical, as for the HGMF axial filter.

5. CONCLUSIONS

The analysis of the HGMF configurations with bound flow field was meant to solve two important problems met in the magnetic filtration process: getting the maximum filtering efficiency and extending the utilization duration of the equipment by placing the ferromagnetic wires outside the flow space, thus performing their anticorrosive and antierosion protection. Our results have been obtained under the condition of some simplifying hypotheses. The fluid suspension was considered diluted, so that the magnetic dipolar interactions and the collisions between particles could be neglected. At the same time, we used for the fluid suspension flow the Hagen–Pouseuille relations for laminar flow in cylindrical tubes with circular cross section in the case of the HGMF axial configuration, and between plane parallel plates in the case of the HGMF transversal configuration, respectively. The designs of magnetic filters described at the end of our work are adequate for the operation in many real situations. This is facilitated by the fact that the filtration efficiency has been analysed depending on all constructive and working parameters of the system. Depending on the practical situation, one can adjust either the magnetic field intensity or the suspension flow velocity, so that to obtain a maximum filtration efficiency. The problem of the HGMF systems with bound flow field remains still open, since their analysis area can be extended by taking into account more complex flow situations for the fluid suspensions, in which the magnetic and hydrodinamic interactions between particles are considered. At the same time, the formation and stability of the particles' buildups, as an actual problem in the study of granular systems, has not been dealt with yet.

REFERENCES

Badescu, V., Murariu, V., Rotariu, O. & Rezlescu, N. 1995a Capture modeling for an axial high gradient magnetic separation filter with a bounded flow field. *Powder Technology* **83**, 259–264.

Badescu, V., Rotariu, O., Murariu, V. & Rezlescu, N. 1995b Magnetic capture modelling for a transversal high gradient filter cell with bounded flow field. *Int. J. Appl. Electromagnetics and Mechanics* (to appear).

Elliott, H. H., Holloway, J. H. & Abbott, D. G. 1979 The potential uses of high gradient magnetic filtration for high temperature water purification in boiling water reactors. In *Industrial Applications of Magnetic Separation* (Edited by Y. A. Liu). IEEE. Pub. No. 78CH1447-2 MAG, New York, 1979, pp. 127–133.

Oberteuffer, J. A. 1974 Magnetic separation: a review of principles, devices and applications. *IEEE Trans. Magn.* **10**, 223–238.

Sushil, K. & Ernest, G. 1979 A pilot-scale study of condensate-feedwater polishing by high gradient magnetic filtration (HGMF). In *Industrial Applications of Magnetic Separation* (Edited by Y. A. Liu). IEEE. Pub. No. 78CH1447-2 MAG, New York, 1979, pp. 121–126.

Watson, J. P. H. 1973 Magnetic filtration. *J. Appl. Phys.* **44**, 4209–4213.